Available online at www.sciencedirect.com
ScienceDirect
Journal of Sound and Vibration 318 (2008) 206–226
JOURNAL OF SOUND AND VIBRATION
www.elsevier.com/locate/jsvi

Structural waveguide behaviour of a beam–plate system

D.J. Thompson*, N.S. Ferguson, J.W. Yoo, J. Rohlfing

Institute of Sound and Vibration Research, University of Southampton, Southampton SO17 1BJ, UK

Received 29 October 2007; received in revised form 5 March 2008; accepted 8 April 2008
Handling Editor: C.L. Morfey
Available online 22 May 2008

Abstract

Structures which have a constant cross-section normal to a longitudinal axis can be considered as waveguides in which vibration can propagate in the form of various waves in the longitudinal direction. The dynamic behaviour of such systems can be found by using a Fourier transform approach in terms of wavenumbers in the longitudinal direction. Analytical solutions are available for simple, infinitely long waveguides, whereas for more complex waveguides numerical approaches have been developed using finite element techniques to describe the cross-section. In the present paper an analytical Fourier transform approach is used to find the dynamic behaviour of a system consisting of two parallel beams coupled by a plate, when a point force is applied to one of the beams. Multiple waves occur in the longitudinal direction, the number of waves depending on the number of modes of the equivalent cross-section. However, the motion of the driven beam is shown to be dominated by the contribution from only one or two waves at each frequency, these having wavenumbers closest to that of the uncoupled beam. The motion of the plate is also shown to be dominated by these wavenumbers for excitation on the beam. Experimental results are obtained on beam–plate–beam systems with identical and non-identical beams, which show good agreement with the predictions. In particular, these confirm that the plate response is dominated by waves with wavenumbers in the beam direction that follow those of the excited beam.

1. Introduction

Structures which have a constant geometry along one coordinate direction (here denoted as the x-direction) may be considered as waveguides. Examples include beams, pipes, bridges, extruded panels and many beam–stiffened plate structures such as ship and aircraft structures. As such structures become long in the x-direction (or as frequency increases), the use of conventional techniques to find their vibration behaviour, for example finite element analysis, becomes impractical. Instead, a wave approach can be used, making direct use of the two-dimensional (2D) geometry. Wave solutions can be sought in the x-direction whilst the cross-section may be modelled either analytically or using special finite elements.

Waveguides are well known in acoustics, where a duct of constant cross-section permits a series of waves to propagate without attenuation. At low frequency only the lowest order wave (a plane wave) can propagate; as the frequency is increased, successive higher modes start to propagate [1]. Each propagating wave corresponds

*Corresponding author. Tel.: +44 23 8059 2510; fax: +44 23 8059 3190.
E-mail address: djt@isvr.soton.ac.uk (D.J. Thompson).

0022-460X/$ - see front matter © 2008 Elsevier Ltd. All rights reserved.
doi:10.1016/j.jsv.2008.04.011

to a mode of the cross-section; these waves 'cut on' at a frequency corresponding to the resonance frequency of the 2D system. Similar phenomena occur for electromagnetic waveguides (e.g. Ref. [2]).

An infinite beam forms a simple structural waveguide sustaining bending, torsional and extensional waves. In Ref. [3] the free wave propagation is determined for two parallel beams (or plates) in bending coupled by an elastic layer. In this case a single propagating wave exists at low frequency. Above a transition frequency, identified as the resonance of the mass of the two beams on the stiffness of the interlayer, a second propagating wave also exists. The wavenumbers of these two waves tend to those of the uncoupled beams at high frequency.

Another simple structural waveguide considered in Ref. [3] consists of an infinitely long plate strip with parallel sliding boundaries. The vibration of this system is solved as a sum of modal contributions across the width and in terms of the longitudinal wavenumber. At low frequency only a single wave type with a constant deflection across the plate width can propagate and the system behaves like a beam. As frequency increases, waves of progressively higher order occur. These commence at frequencies corresponding to resonances of the cross-section, in this case given by $k_pL = n\pi$, where k_p is the plate-free wavenumber, L is the width and n is an integer. A Fourier transform with respect to the wavenumber in the longitudinal direction allows the point mobility to be obtained.

Fourier transform approaches are widely used in analysing the vibration of an infinite layered ground, both for seismological applications [4] and for studying the vibration induced by trains [5]. These mostly use a 2D Fourier transform in terms of the wavenumbers in two perpendicular directions parallel to the ground surface. In the case of a railway track on a ground [5] the waves in the track are modified by the presence of the ground. Ji [6] used a similar Fourier transform approach to model an infinite beam coupled to an infinite plate and subsequently developed a hybrid Fourier transform approach for the case of a finite beam attached to an infinite plate [6,7].

In recent years, the spectral or wavenumber finite element method has been developed for application to structural waveguides [8–11]. In this, the 2D cross-section is represented by special finite elements whilst in the third dimension wave solutions are assumed. Solutions may be obtained for the free wavenumbers by solving the dispersion equation and the forced response may be found by using a Fourier integral over a range of real-valued wavenumbers. Applications have included railway tracks [12,13], pipes [14] and car tyres [15].

An alternative numerical approach [16,17] is to represent a small segment of the structure in the x-direction using conventional finite elements and to invoke periodic structure theory [18] to represent wave propagation in an infinite structure. This has the advantage of allowing the use of conventional finite elements, whereas the spectral finite element method described above requires higher order stiffness matrices in addition to the conventional mass and stiffness matrices. On the other hand, an approximation is introduced in the x-direction (dependent on the finite element shape function) whereas the other methods discussed above work with exact wave solutions.

In this paper, the Fourier transform approach is used with analytical models, firstly of two beams connected by a resilient layer and then of a finite width plate strip with two parallel beams attached along the long edges. This latter problem is treated initially by assuming that the beams are infinitely stiff to torsion and thus the plate edges at the junction are effectively sliding. The effect of this simplification is also investigated. The present work is limited to relatively low frequencies where the beams and plate behave simply in bending (and torsion) without deformation of their cross-sections. Such structures are simple enough to allow analytical modelling of the cross-section, allowing insight to be gained into their behaviour. Wavenumber or spectral finite elements could also have been used for such a problem; the present analytical solutions could be considered as a benchmark for such models.

It is shown that there are, in general, many wave solutions in the x-direction, but that the solution closest to the wavenumber of the driven beam tends to dominate the response of the driven beam and also of the plate. Example calculations are given for cases where the two beams are identical as well as where they have different free wavenumbers.

Experimental results on finite length waveguides are presented for comparison with the analytical results. A wavenumber correlation technique [19,20] is used to extract the dominant wavenumbers in the plate and beams. This analysis is used to verify experimentally that, for excitation on one of the beams, the wavenumbers in the plate in the x-direction follow those of the driven beam.

2. Two beams connected by resilient layer

2.1. Fourier transform approach

As a preliminary to considering the beam–plate system, a simple waveguide structure is considered, consisting of two infinite Euler–Bernoulli beams connected by a resilient layer of stiffness s per unit length, as shown in Fig. 1. Solutions for the coupled waves in this case are given in Ref. [3], but the motion of this system will be found here using the Fourier transform approach, as this will assist in interpretation of the more complex cases considered later. Harmonic motion at frequency ω is assumed. Spatial Fourier transform pairs are defined by the relationship between the longitudinal coordinate x and real wavenumber k_x in the x-direction,

$$\tilde{W}_i(k_x) = \int_{-\infty}^{\infty} \tilde{w}_i(x)\, \mathrm{e}^{-\mathrm{i}k_x x}\, \mathrm{d}x \tag{1}$$

$$\tilde{w}_i(x) = \frac{1}{2\pi} \int_{-\infty}^{\infty} \tilde{W}_i(k_x)\, \mathrm{e}^{\mathrm{i}k_x x}\, \mathrm{d}k_x \tag{2}$$

where $\tilde{w}_i$ is the complex displacement amplitude, $\tilde{W}_i$ is the Fourier transformed displacement and subscript $i = 1, 2$ represent the two beams ($\tilde{}$ indicates complex quantities).

The resilient layer applies a force per unit length $\tilde{f}_1(x)$ downwards on beam 1 and an identical but opposite force, for convenience denoted $\tilde{f}_2(x) = -\tilde{f}_1(x)$, on beam 2, as shown in Fig. 1. An external point force $\tilde{F}_0\delta(x-0)$ acts at $x = 0$. The equation of motion of beam 1, including damping is

$$\tilde{D}_{b1} \frac{\mathrm{d}^4 \tilde{w}_{b1}}{\mathrm{d}x^4} - m'_{b1}\omega^2 \tilde{w}_{b1} = \tilde{F}_0 \delta(x-0) - \tilde{f}_1(x) \tag{3}$$

where $\tilde{w}_{b1}$ is the complex displacement amplitude, $\tilde{D}_{b1}$ is the complex bending stiffness (i.e. including damping via a factor $(1+\mathrm{i}\eta)$, where η is the loss factor) and m'_{b1} is the mass per unit length. The corresponding spatial Fourier transform becomes

$$\tilde{D}_{b1} k_x^4 \tilde{W}_{b1}(k_x) - m'_{b1}\omega^2 \tilde{W}_{b1}(k_x) = \tilde{F}_0 - \tilde{F}_1(k_x) \tag{4}$$

and similarly for beam 2, on which no external force acts,

$$\tilde{D}_{b2} k_x^4 \tilde{W}_{b2}(k_x) - m'_{b2}\omega^2 \tilde{W}_{b2}(k_x) = -\tilde{F}_2(k_x) \tag{5}$$

where subscripts $b1$ and $b2$ stand for beams 1 and 2, while $\tilde{F}_1(k_x)$ and $\tilde{F}_2(k_x)$ are the Fourier transforms of $\tilde{f}_1(x)$ and $\tilde{f}_2(x)$, respectively. The forces are related to the beam displacements according to the stiffness matrix of the resilient layer

$$\begin{Bmatrix} \tilde{F}_1(k_x) \\ \tilde{F}_2(k_x) \end{Bmatrix} = \begin{bmatrix} s & -s \\ -s & s \end{bmatrix} \begin{Bmatrix} \tilde{W}_{b1}(k_x) \\ \tilde{W}_{b2}(k_x) \end{Bmatrix} \tag{6}$$

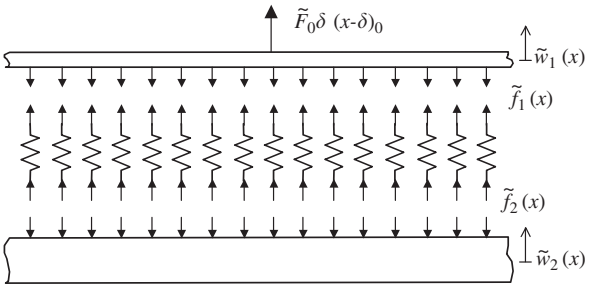

Fig. 1. Two beams connected by a resilient layer.

This can be combined with Eqs. (4) and (5) to eliminate the internal forces $\tilde{F}_1(k_x)$ and $\tilde{F}_2(k_x)$ giving

$$(\mathbf{\Gamma}+\mathbf{S})\begin{Bmatrix}\tilde{W}_{b1}(k_x)\\ \tilde{W}_{b2}(k_x)\end{Bmatrix}=\begin{Bmatrix}\tilde{F}_0\\ 0\end{Bmatrix} \tag{7}$$

where $\mathbf{S}$ denotes the stiffness matrix in Eq. (6) and $\mathbf{\Gamma}$ is a diagonal matrix containing the terms

$$\gamma_{11}=\tilde{D}_{b1}k_x^4-m'_{b1}\omega^2,\quad \gamma_{22}=\tilde{D}_{b2}k_x^4-m'_{b2}\omega^2 \tag{8}$$

By evaluating the inverse of $(\mathbf{\Gamma}+\mathbf{S})$ explicitly, the response of the driven beam can be found as

$$\tilde{W}_{b1}(k_x)=\frac{\tilde{F}_0}{\tilde{D}_{b1}}\frac{k_x^4-\tilde{k}_{b2}^4+s/\tilde{D}_{b2}}{\left(k_x^4-\tilde{k}_{b1}^4+s/\tilde{D}_{b1}\right)\left(k_x^4-\tilde{k}_{b2}^4+s/\tilde{D}_{b2}\right)-s^2/(\tilde{D}_{b1}\tilde{D}_{b2})} \tag{9}$$

where $\tilde{k}_{bi}=\left(\omega^2 m'_{bi}/\tilde{D}_{bi}\right)^{1/4}$ are the wavenumbers in the uncoupled beams. Similarly, the response of the non-driven beam becomes

$$\tilde{W}_{b2}(k_x)=\frac{\tilde{F}_0}{\tilde{D}_{b1}}\frac{s/\tilde{D}_{b2}}{\left(k_x^4-\tilde{k}_{b1}^4+s/\tilde{D}_{b1}\right)\left(k_x^4-\tilde{k}_{b2}^4+s/\tilde{D}_{b2}\right)-s^2/(\tilde{D}_{b1}\tilde{D}_{b2})} \tag{10}$$

For an undamped system, the free wavenumbers of the coupled system correspond to the zeros of the denominator of Eqs. (9) and (10), i.e. the solutions of

$$(k_x^4-k_{b1}^4+s/D_{b1})(k_x^4-k_{b2}^4+s/D_{b2})-s^2/(D_{b1}D_{b2})=0 \tag{11}$$

where k_{bi} and D_{bi} are real in the absence of damping. At high frequencies s has negligible effect and the solutions tend towards the free wavenumbers of the two beams, k_{bi}. At low frequencies only one propagating wave exists; the cut-on frequency of the second wave can be found by setting $k_x=0$ in Eq. (11). Substituting for k_{bi} this yields

$$\omega_0^2=\frac{s}{m'_{b1}}+\frac{s}{m'_{b2}} \tag{12}$$

from which it is clear that the cut-on frequency ω_0 corresponds to the resonance of the two beam masses on the resilient layer.

2.2. Results

Results are presented for three configurations. They are chosen to correspond to the beam configurations included in the measurements in Section 4. In one configuration the two beams are identical, while in the other two their widths are identical but their heights (and therefore masses) are in the ratio 1:2.364, corresponding to a wavenumber ratio k_{b2}/k_{b1} of 0.650 or 1.537 depending which beam is excited.

The free wavenumbers (for the undamped case), found from Eq. (11), are shown in Fig. 2. The frequency is normalised by ω_0 (see Eq. (12)) and the wavenumber is normalised by $k_0=k_{b1}(\omega_0)$.

At low frequency a single wavenumber is present corresponding to the composite structure vibrating as a single beam. At $\omega=\omega_0$ the second wave cuts on and tends towards the free wavenumber of the stiffer beam. Meanwhile, the wave already present tends towards the free wavenumber of the less stiff beam. For the case of identical beams the higher wavenumber solution is identically equal to k_{bi} for all frequencies.

The response amplitude in the wavenumber domain, $|\tilde{W}_{b1}(k_x)|$, is plotted against frequency and wavenumber k_x in Fig. 3(a) for the two identical beams. Fig. 3(b) shows the corresponding response of the non-driven beam, $|\tilde{W}_{b2}(k_x)|$. Equivalent results are given for the two dissimilar beam cases in Fig. 3(c)–(f). Areas of dark shading correspond to large magnitudes. These are normalised by the maximum response at each frequency. The loss factor was set to 0.005 in these examples for clarity of the results.

Comparing these results with Fig. 2 it can be seen that, above ω_0, the region of maximum response on the driven beam follows the wave closest to the free wavenumber of that beam in each case. However, the response

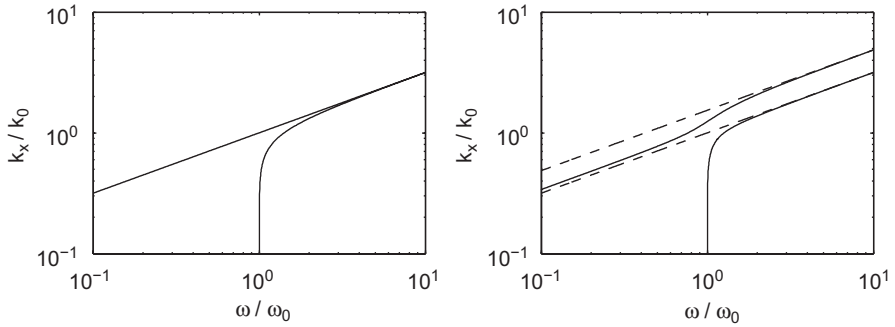

Fig. 2. Free wave solutions for undamped case of two beams connected by resilient layer. Frequency normalised by cut-on frequency ω_0, wavenumber by k_{b1} at ω_0: (a) identical beams, (b) dissimilar beams ($b1$ is the stiffer beam). (—) Coupled beam wavenumbers and (– – –) uncoupled beam wavenumbers.

of the non-driven beam is dominated by the wavenumber of the stiffer beam (for dissimilar beams), whichever beam is excited. Note that Figs. 3(d) and (f) are identical, as Eq. (10) is unchanged if the subscripts $b1$ and $b2$ are exchanged.

Fig. 4 shows the point mobility for each case, found from the inverse Fourier transform of Eq. (9) at $x = 0$, in this case with the damping loss factor set to 0.05. In each case the mobility has been normalised by the mobility of beam 1, Y_{b1}, at ω_0. At low frequency the results correspond to a composite beam. A peak is found at the cut-on frequency of the second wave, above which the mobility tends to Y_{b1}.

Finally, the degree of isolation afforded by the resilient layer is assessed by evaluating the ratio of the summed squared vibration on each beam. Using Parseval's identity this can be found from the Fourier transform:

$$E_i = \int_{-\infty}^{\infty} \left|\tilde{w}_i(x)\right|^2 \mathrm{d}x = \frac{1}{2\pi} \int_{-\infty}^{\infty} \left|\tilde{W}_i(k_x)\right|^2 \mathrm{d}k_x \tag{13}$$

Fig. 5 shows the ratio E_2/E_1 for the three configurations considered, again with the damping loss factor set to 0.05. For identical beams the two beams have almost equal average vibration for frequencies up to $3\omega_0$, whereas for dissimilar beams the degree of isolation is much greater at high frequency due to the mismatch in their free wavenumbers. When the stiffer beam is driven the ratio resembles closely that of a single degree-of-freedom isolator, but when the less stiff beam is driven the isolation above ω_0 is much greater, in this case by about a factor of 10. Even below ω_0 the ratio E_2/E_1 is less than unity as the response of the driven beam is higher in this case.

3. Beam–plate–beam system

3.1. Fourier transform solution

Consider now the waveguide structure consisting of two infinite beams connected by an infinitely long, finite width plate, as shown in Fig. 6, which is the main subject of this paper. As above, harmonic motion at frequency ω is assumed. The beams are represented as Euler–Bernoulli beams and the plate is assumed to be thin and isotropic. These models are valid for frequencies where $kh < 1$, where h is the height of the beam or plate. In-plane plate motion is also neglected. At this stage, for simplicity, the beams are assumed to be infinitely stiff to torsion along $y = 0$ and L_y. They are also assumed to be joined to the plate at their common neutral axis. The effect of the first of these assumptions will be considered later.

The forces $\tilde{f}_1(x)$ and $\tilde{f}_2(x)$ per unit length act between the plate and beams 1 and 2 respectively, as shown in Fig. 6, and an external point force $\tilde{F}_0\delta(x-0)$ acts on beam 1 at $x = 0$. The motion of the beams is as given by Eqs. (4) and (5).

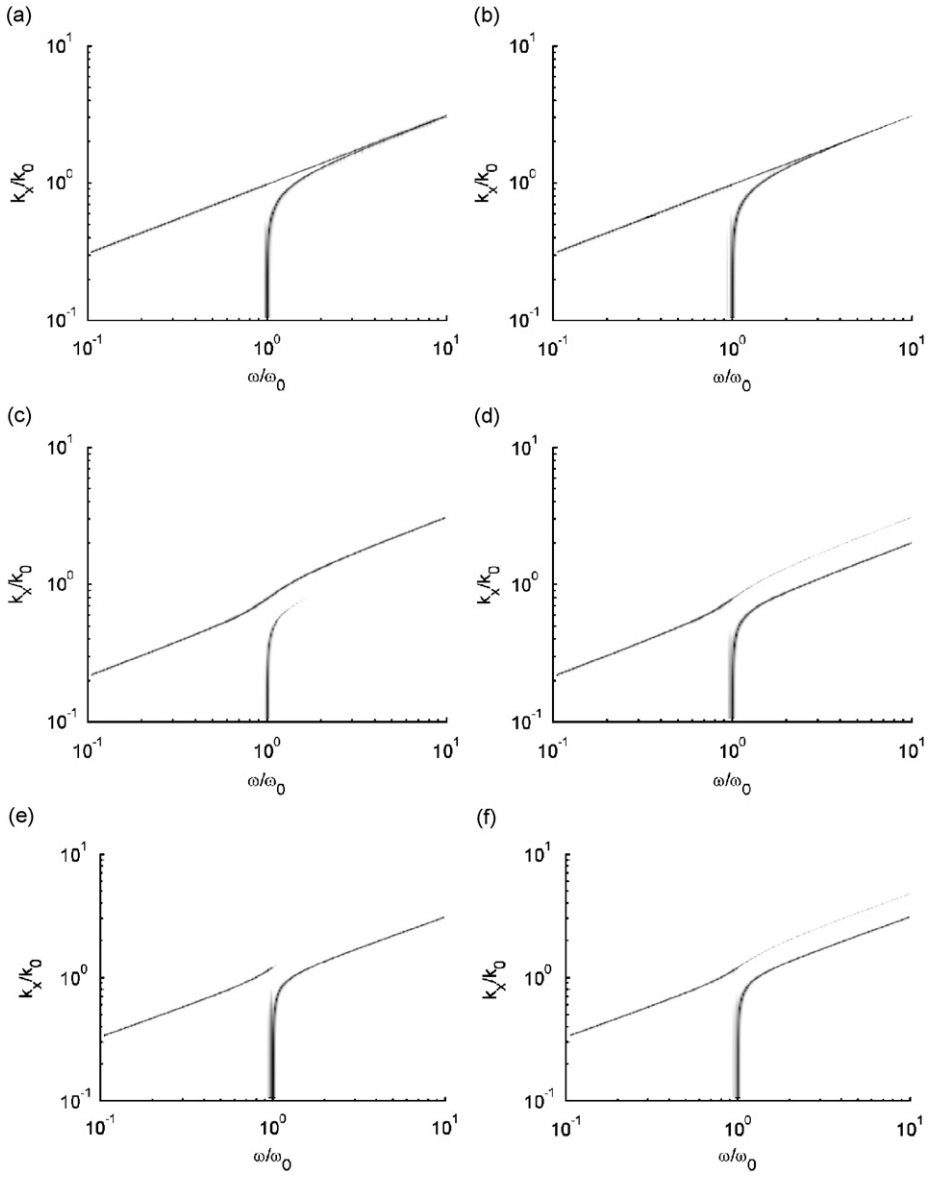

Fig. 3. Magnitude of response in wavenumber–frequency domain of two beams connected by resilient layer. Response normalised to maximum at each frequency, dynamic range 25 dB. Left: on driven beam, right: on non-driven beam. (a,b) Identical beams, (c,d) less stiff beam is driven and (e,f) stiffer beam is driven.

It is now necessary to find the dynamic stiffness matrix of the plate at wavenumber k_x. The Fourier transformed equation of motion of the plate including damping is

$$\tilde{D}_p\left(k_x^4\tilde{W}_p(k_x,y)-2k_x^2\frac{\partial^2\tilde{W}_p(k_x,y)}{\partial y^2}+\frac{\partial^4\tilde{W}_p(k_x,y)}{\partial y^4}\right)-m_p''\omega^2\tilde{W}_p(k_x,y)=0 \tag{14}$$

where $\tilde{D}_p$ is the complex plate bending stiffness and m_p'' is its mass per unit area. For a given real value of k_x, solutions for waves in the plate can be assumed of the form $\tilde{B}_i\,e^{\tilde{\gamma}_{yi}y}$, where $\tilde{\gamma}_{yi}$ is the propagation coefficient in the plate in the direction normal to the beam (according to this definition *imaginary* values of $\tilde{\gamma}_{yi}$ represent propagating waves). To find $\tilde{\gamma}_{yi}$ it is helpful to define $\tilde{k}_p$ as the damped free wavenumber in the plate, given by $\tilde{k}_p=\left(\omega^2m_p''/\tilde{D}_p\right)^{1/4}$. The propagation coefficients in the plate in the y direction are found from

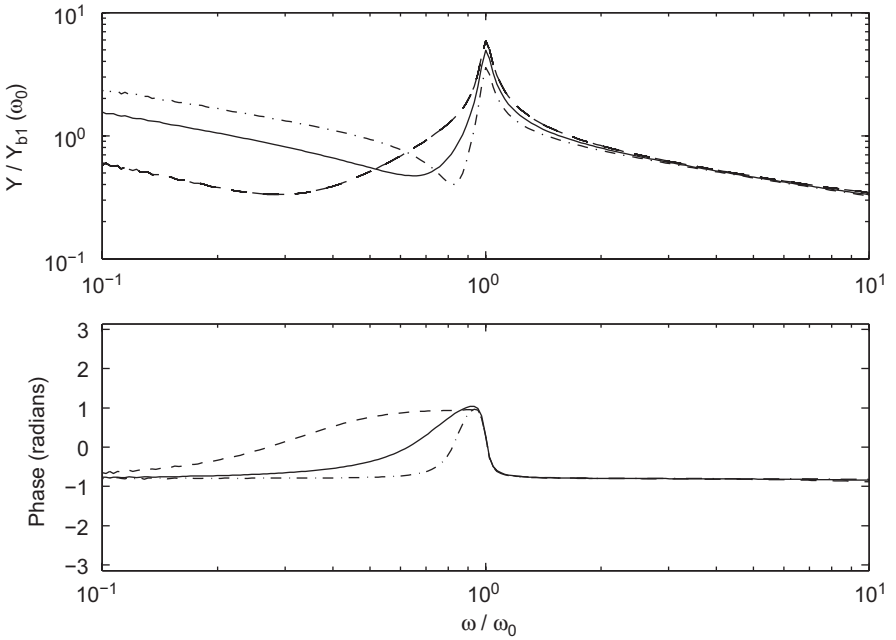

Fig. 4. Point mobility of two infinite beams connected by a resilient layer. The mobility is normalised by that of the driven beam at frequency ω_0: (—) identical beams, (– · – ·) stiffer beam driven and (– – –) less stiff beam driven.

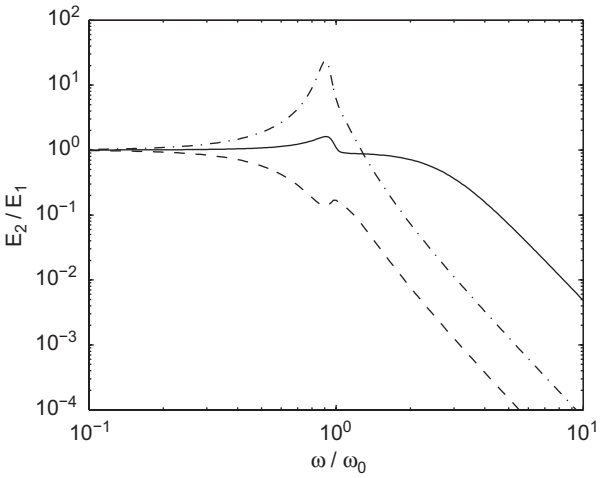

Fig. 5. Ratio of total energy in the non-driven beam to that in the driven beam for two beams connected by a resilient layer: (—) identical beams, (– · – ·) stiffer beam driven and (– – –) less stiff beam driven.

Eq. (14) to be

$$\tilde{\gamma}_{yi} = \pm\sqrt{k_x^2 - \tilde{k}_p^2} = \pm\tilde{\gamma}_{y1} \text{ and } \tilde{\gamma}_{yi} = \pm\sqrt{k_x^2 + \tilde{k}_p^2} = \pm\tilde{\gamma}_{y2} \tag{15}$$

If $|k_x| < |\tilde{k}_p|$, then the terms $\pm\tilde{\gamma}_{y1}$ are predominantly imaginary and represent propagating waves and $\pm\tilde{\gamma}_{y2}$ are predominantly real and are therefore nearfield waves. Conversely, if $|k_x| > |\tilde{k}_p|$, all four waves have large real and imaginary parts and behave as nearfield waves. The motion of the plate can be written as

$$\tilde{W}_p(k_x, y) = \tilde{B}_1 \, e^{\tilde{\gamma}_{y1} y} + \tilde{B}_2 \, e^{\tilde{\gamma}_{y2} y} + \tilde{B}_3 \, e^{-\tilde{\gamma}_{y1} y} + \tilde{B}_4 \, e^{-\tilde{\gamma}_{y2} y} \tag{16}$$

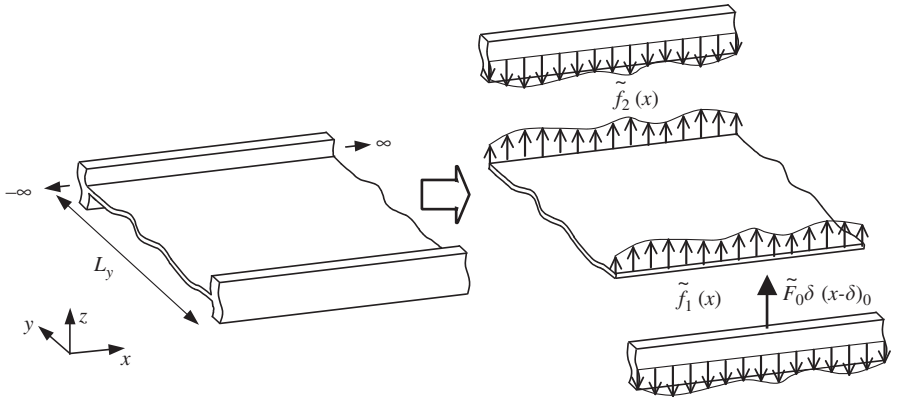

Fig. 6. Two infinite beams coupled to an infinite plate strip of finite width. The beams are constrained not to rotate.

The displacement and rotation at the plate edges are equal to those of the corresponding beam, giving

$$\begin{Bmatrix} \tilde{W}_{b1} \\ \tilde{W}_{b2} \\ \tilde{\Theta}_{b1} \\ \tilde{\Theta}_{b2} \end{Bmatrix} = \begin{bmatrix} 1 & 1 & 1 & 1 \\ e^{\tilde{\gamma}_{y1}L_y} & e^{\tilde{\gamma}_{y2}L_y} & e^{-\tilde{\gamma}_{y1}L_y} & e^{-\tilde{\gamma}_{y2}L_y} \\ \tilde{\gamma}_{y1} & \tilde{\gamma}_{y2} & -\tilde{\gamma}_{y1} & -\tilde{\gamma}_{y2} \\ \tilde{\gamma}_{y1}e^{\tilde{\gamma}_{y1}L_y} & \tilde{\gamma}_{y2}e^{\tilde{\gamma}_{y2}L_y} & -\tilde{\gamma}_{y1}e^{-\tilde{\gamma}_{y1}L_y} & -\tilde{\gamma}_{y2}e^{-\tilde{\gamma}_{y2}L_y} \end{bmatrix} \begin{Bmatrix} \tilde{B}_1 \\ \tilde{B}_2 \\ \tilde{B}_3 \\ \tilde{B}_4 \end{Bmatrix} = \mathbf{C}_1 \begin{Bmatrix} \tilde{B}_1 \\ \tilde{B}_2 \\ \tilde{B}_3 \\ \tilde{B}_4 \end{Bmatrix} \tag{17}$$

where $\tilde{\Theta}_{bi}$ is the amplitude of the rotation. Similarly the forces and moments at the plate edges are given by

$$\begin{Bmatrix} \tilde{F}_1 \\ \tilde{F}_2 \\ \tilde{M}_1 \\ \tilde{M}_2 \end{Bmatrix} = \tilde{D}_p \begin{bmatrix} p_1 & p_2 & -p_1 & -p_2 \\ -p_1 e^{\tilde{\gamma}_{y1}L_y} & -p_2 e^{\tilde{\gamma}_{y2}L_y} & p_1 e^{-\tilde{\gamma}_{y1}L_y} & p_2 e^{-\tilde{\gamma}_{y2}L_y} \\ -q_1 & -q_2 & -q_1 & -q_2 \\ q_1 e^{\tilde{\gamma}_{y1}L_y} & q_2 e^{\tilde{\gamma}_{y2}L_y} & q_1 e^{-\tilde{\gamma}_{y1}L_y} & q_2 e^{-\tilde{\gamma}_{y2}L_y} \end{bmatrix} \begin{Bmatrix} \tilde{B}_1 \\ \tilde{B}_2 \\ \tilde{B}_3 \\ \tilde{B}_4 \end{Bmatrix} = \mathbf{C}_2 \begin{Bmatrix} \tilde{B}_1 \\ \tilde{B}_2 \\ \tilde{B}_3 \\ \tilde{B}_4 \end{Bmatrix} \tag{18}$$

where $p_i = \tilde{\gamma}_{yi}^3 - (2-\nu)\tilde{\gamma}_{yi}k_x^2$, $q_i = \tilde{\gamma}_{yi}^2 - \nu k_x^2$, ν is Poisson's ratio and $\tilde{M}_i$ is the moment per unit length. This allows a dynamic stiffness matrix for the plate to be determined for wavenumber k_x

$$\begin{Bmatrix} \tilde{F}_1 \\ \tilde{F}_2 \\ \tilde{M}_1 \\ \tilde{M}_2 \end{Bmatrix} = \mathbf{S}(k_x) \begin{Bmatrix} \tilde{W}_{b1} \\ \tilde{W}_{b2} \\ \tilde{\Theta}_{b1} \\ \tilde{\Theta}_{b2} \end{Bmatrix} \tag{19}$$

where $\mathbf{S}$ is given by

$$\mathbf{S}(k_x) = \mathbf{C}_2\mathbf{C}_1^{-1} \tag{20}$$

Assuming sliding conditions for the edges of the plate, as the beams are assumed infinitely stiff to torsion, the rotation on the edge, $\tilde{\Theta}_{bi}$, is zero. Thus only the first two rows and columns of $\mathbf{S}$ are required. In a similar way to Eq. (9) the response of the driven beam can be expressed as

$$\tilde{W}_{b1}(k_x) = \frac{\tilde{F}_0}{\tilde{D}_{b1}} \frac{k_x^4 - \tilde{k}_{b2}^4 + s_{22}/\tilde{D}_{b2}}{(k_x^4 - \tilde{k}_{b1}^4 + s_{11}/\tilde{D}_{b1})(k_x^4 - \tilde{k}_{b2}^4 + s_{22}/\tilde{D}_{b2}) - s_{12}s_{21}/(\tilde{D}_{b1}\tilde{D}_{b2})} \tag{21}$$

where s_{ij} are elements of the frequency-dependent plate dynamic stiffness matrix, $\mathbf{S}$. Similarly, the response of the non-driven beam becomes

$$\tilde{W}_{b2}(k_x) = \frac{\tilde{F}_0}{\tilde{D}_{b1}} \frac{-s_{21}/\tilde{D}_{b2}}{(k_x^4 - \tilde{k}_{b1}^4 + s_{11}/\tilde{D}_{b1})(k_x^4 - \tilde{k}_{b2}^4 + s_{22}/\tilde{D}_{b2}) - s_{12}s_{21}/(\tilde{D}_{b1}\tilde{D}_{b2})} \tag{22}$$

The response of the plate can be found via the coefficients $\tilde{B}_i$ using Eqs. (16) and (17). The response of the plate and beams can subsequently be found in spatial coordinates by use of the inverse Fourier transform, given in Eq. (2).

3.2. Determination of wavenumbers in the undamped system

It is of interest to identify wave solutions which propagate freely in the x-direction for an undamped system. Such solutions can be found by setting the denominator of Eq. (21) to zero. Results are presented for two beam–plate–beam configurations, the relevant parameters of which are listed in Table 1 in the form of wavenumber ratios and mass ratios. These correspond to the experimental configurations considered in Section 4 below. The beams have identical widths, so their heights are proportional to k_{bi}^{-2}. In one configuration the two beams are identical; in the other they are dissimilar. The beams are stiffer than the plate, having free wavenumbers ranging between 1/5 and 1/3 of the plate free wavenumber.

Fig. 7(a) shows the wavenumbers k_x for which free wave propagation can occur for the dissimilar beam case. The results are shown against non-dimensional frequency ω/ω_1 where $\omega_1 = (\tilde{D}_p/m_p'')^{1/2}(\pi/L_y)^2$ is the first natural frequency of a plate strip of length L_y with sliding end conditions. This non-dimensional frequency may also be written as $(k_p L_y/\pi)^2$. The wavenumber k_x is shown normalised by π/L_y, the plate-free wavenumber at ω_1. Also shown are the plate and beam free wavenumbers.

At low frequency a single wavenumber is present corresponding to the whole system vibrating as a beam. As frequency increases, successive waves cut on which tend initially towards the free wavenumber of the stiffer beam. Meanwhile, waves already present tend first towards the free wavenumber of the less stiff beam and finally towards the plate-free wavenumber. As the wavenumbers approach the plate wavenumber, several waves occur close together and it becomes more difficult to identify all poles of Eq. (21).

Fig. 7(b) shows equivalent results for the case with two identical beams. Similar behaviour is found, except that as the two beam free wavenumbers are identical there are usually two waves close to the beam wavenumber. One of these will be symmetric with respect the plate centreline, the other anti-symmetric.

3.3. Wave cut-on frequencies

Setting $k_x = 0$ in Eq. (21) allows identification of the cut-on frequency of each wave, the frequency above which free wave propagation occurs. Noting that $\tilde{k}_{bi} = \left(\omega^2 m_{bi}'/\tilde{D}_{bi}\right)^{1/4}$, Eq. (21) reduces to

$$\tilde{W}_{b1}(0) = \tilde{F}_0 \frac{-\omega^2 m_{b2}' + s_{22}}{(-\omega^2 m_{b1}' + s_{11})(-\omega^2 m_{b2}' + s_{22}) - s_{12}s_{21}} \tag{23}$$

This corresponds to the solution for a plate strip (effectively a beam) with end masses, in which the dynamic stiffness matrix of Eq. (20) is now given purely in terms of the free plate wavenumber, i.e. $\tilde{\gamma}_{y1} = \mathrm{i}\tilde{k}_p$ and $\tilde{\gamma}_{y2} = \tilde{k}_p$.

The corresponding natural frequencies, the poles of Eq. (23), are listed in Table 2 for three cases: the two identical beams, the two dissimilar beams and a case with the most flexible of the three beams on one side and a clamped boundary on the other. These are given in the form ω/ω_1, where ω_1 is the natural frequency of the plate strip with sliding boundaries. Due to the effect of the added mass of the beams, the first modes in each

Table 1
Beam–plate–beam configurations considered (all beams have the same width)

	Identical beams	Dissimilar beams	
		Smaller beam	Larger beam
k_{b1}/k_p	0.260	0.313	0.204
k_{b1}/k_{b2}	1	0.650	1.537
$m_{b1}'/m_p'' L_y$	0.333	0.229	0.542

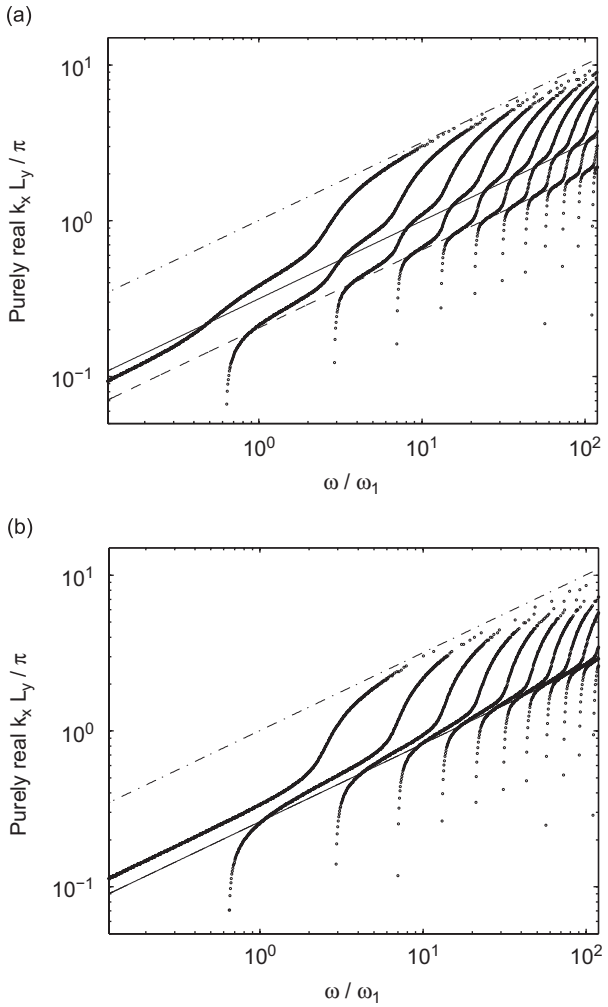

Fig. 7. Real wavenumbers k_x for plate with two beams and damping set to zero: (– · – ·) free wavenumber in plate, (—) free wavenumber in less stiff beam, (– – –) free wavenumber in stiffer beam, (●●●●●) wavenumbers of coupled system: (a) dissimilar beams and (b) identical beams.

Table 2
Natural frequencies of plate strip with end masses and sliding boundaries expressed as ω/ω_1, where ω_1 is the natural frequency of a plate strip of identical length with sliding ends

Identical beams	Dissimilar beams	Smaller beam plus clamped edge
0.653	0.639	0.416
2.957	2.940	2.611
7.098	7.086	6.676
13.18	13.18	12.72
21.17	21.17	20.74
31.28	31.28	30.76

case are lower than ω_1. Higher order modes tend towards $(n-\frac{1}{2})^2\omega_1$, which is indicative of clamped boundaries. This occurs because the impedance of the added mass becomes much larger than that of the plate strip and restrains the translation, the rotation already being constrained by the sliding boundary conditions. These frequencies can be seen to correspond to the cut-on frequencies in Fig. 7.

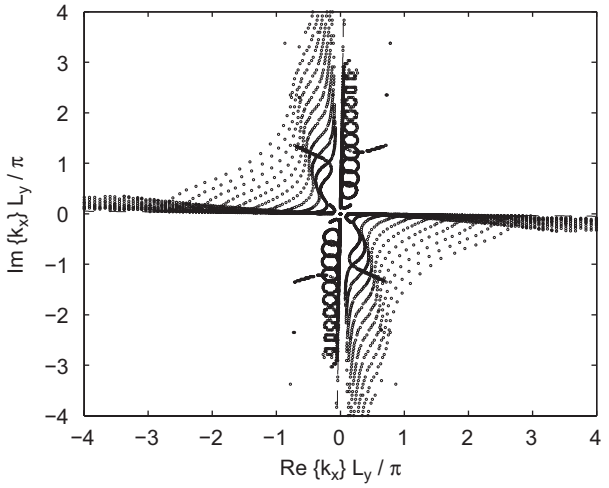

Fig. 8. Wavenumbers k_x plotted on complex plane for the case of two identical beams and structural damping loss factor of 0.05: (– – –) wavenumbers in uncoupled beam or plate, $\mathrm{Im}(k_x) = -\mathrm{Re}(k_x)\eta/4$; (●●●●●) wavenumbers of coupled system.

3.4. Waves for damped system

Although Eq. (21) is given in terms of real values of k_x, for use in the inverse Fourier transform Eq. (2), the equation is also valid for complex values of k_x. As well as the real-valued poles identified in Section 3.2, purely imaginary and other complex poles occur. In the presence of damping, none of the poles occur on the real axis and it is instructive to seek the location of the poles on the complex plane.

Fig. 8 shows results for the case of two identical beams with a damping loss factor, η, of 0.05 applied to both beams and the plate. Points corresponding to the whole frequency range considered in Fig. 7 are shown. These form loci on the complex plane. The results have rotational symmetry about the origin, as waves travelling in positive and negative x directions differ only in the sign of their wavenumber. Waves in the first (and third) quadrant are all strongly evanescent, occurring only above the diagonal $\mathrm{Re}(k_x) = \mathrm{Im}(k_x)$. In the second (and fourth) quadrant, most waves commence close to the imaginary axis and then, at around their cut-on frequency, they move across to the region close to the real axis. They always remain above the line $\mathrm{Im}(k_x) = -\mathrm{Re}(k_x)\eta/4$.

The corresponding real and imaginary parts of the wavenumbers in the second quadrant are shown in Fig. 9 as a function of frequency. The real part shows similar behaviour to that in Fig. 7(b) except that the real part is non-zero below the corresponding cut-on frequency. The imaginary part falls sharply around the cut-on frequency to a value close to $k_{b1}\eta/4$ before rising (as the group velocity falls) and then dropping back to $k_p\eta/4$ as the real part tends towards k_p. Similar results can be obtained for dissimilar beams [21]. As before, not all wavenumber solutions could be found, especially when the real part tends towards the plate free wavenumber.

3.5. Wave contributions to mobility

Although many waves are present in the system, when excited by a point force the response in some waves is greater than in others. In order to illustrate this, the response amplitude in the wavenumber domain, $|\tilde{W}_{b1}(k_x)|$, is plotted against frequency and (real) wavenumber k_x in Fig. 10(a) for the two identical beams. Fig. 10(b) shows the response of the non-driven beam, $|\tilde{W}_{b2}(k_x)|$. Equivalent results are given in Fig. 10(c) and (d) for dissimilar beams with excitation on the less stiff beam and in Fig. 10(e) and (f) for excitation on the stiffer beam. Areas of dark shading correspond to large magnitude.

Comparing these results with those in Fig. 7 it can be seen that the region of maximum response on the driven beam corresponds to the wave that is closest to the free wavenumber of that beam in each case. Similar behaviour was seen for the spring-connected case in Fig. 3. On the non-driven beam, waves that are close to

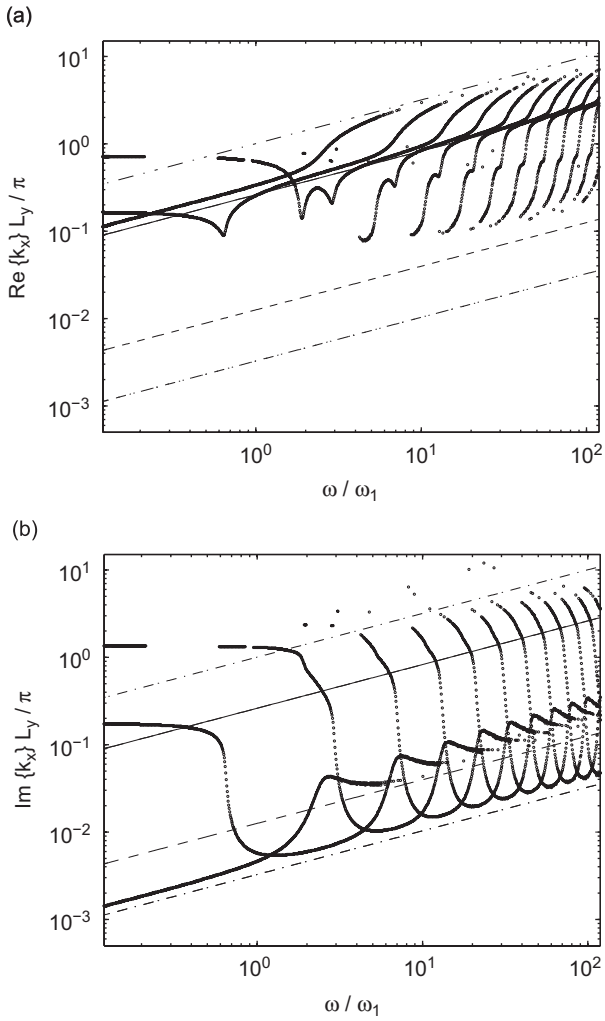

Fig. 9. Wavenumbers k_x from the second quadrant of Fig. 8 for two identical beams: (a) real part, (b) imaginary part. (– · – ·) Free wavenumber in plate, (—) free wavenumber in beams, (– – –) $\eta/4$ times corresponding free wavenumbers, and (●●●●●) wavenumbers of coupled system.

the free wavenumbers of both beams are strongly present, but the wave that is closest to the free wavenumber in the stiffer beam dominates. In all cases the waves that tend towards the free plate wavenumber have negligible contribution to the response of the beams.

Fig. 11 shows the response on the plate at an example position, $y = 0.354L_y$. This again is dominated by the wave closest to the free wavenumber of the driven beam in each case, indicating that the driven beam imposes its behaviour on the more flexible plate. There is negligible contribution from the waves with wavenumbers close to the free plate wavenumber.

3.6. Mobility

The drive point mobility of the three systems is shown in Fig. 12, again for a damping loss factor of 0.05. In each case a set of resonance peaks is seen at similar frequencies, corresponding to the wave cut-on frequencies given in Table 2. These frequencies are determined mainly by the properties of the plate and are only slightly affected by the different beam configurations.

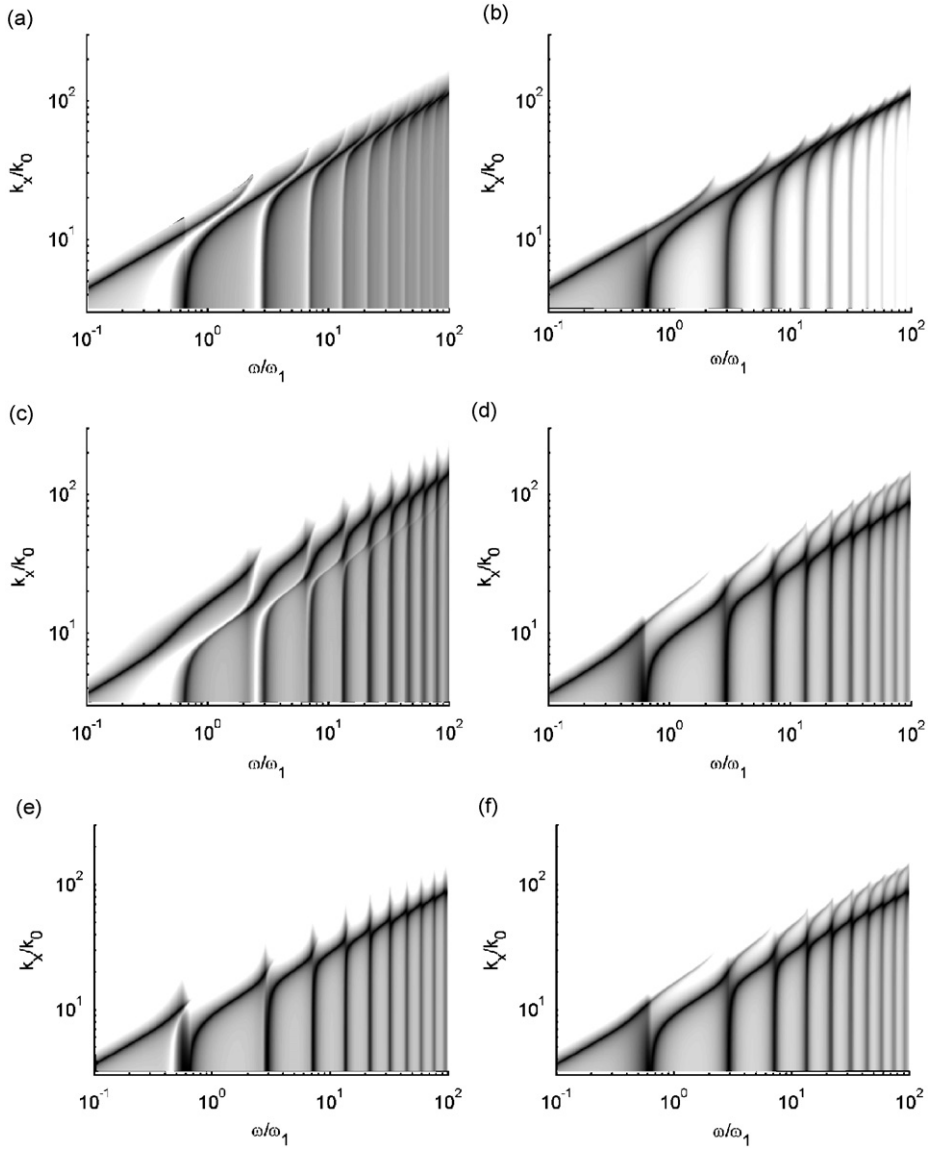

Fig. 10. Magnitude of response in wavenumber–frequency domain of two beams connected by plate. Response normalised to maximum at each frequency, dynamic range 30 dB. Left: on driven beam, right: on non-driven beam: (a,b) identical beams, (c,d) less stiff beam is driven, and (e,f) stiffer beam is driven.

As frequency increases, the mobilities converge towards that of an infinite beam (the driven beam). At lower frequencies the trend is lower, and can be approximated by the mobility of the driven beam connected to a semi-infinite plate [22,23], which are also shown in the figure. At very low frequencies, well below the first resonance, the mobilities tend to that of an equivalent composite beam, corresponding to the single wavenumber seen in Fig. 7.

Fig. 13 shows the ratio of summed squared vibration on each beam, based on Eq. (13). Similar trends are seen to the spring-connected case (Fig. 5). However, the ratios remain close to unity over a wider frequency range because the dynamic stiffness of the plate increases with frequency. The series of peaks seen, particularly for the two dissimilar beam cases, correspond to the anti-resonances in the point mobility. They are thus minima in the energy of the driven beam rather than maxima in the response of the non-driven beam. As for

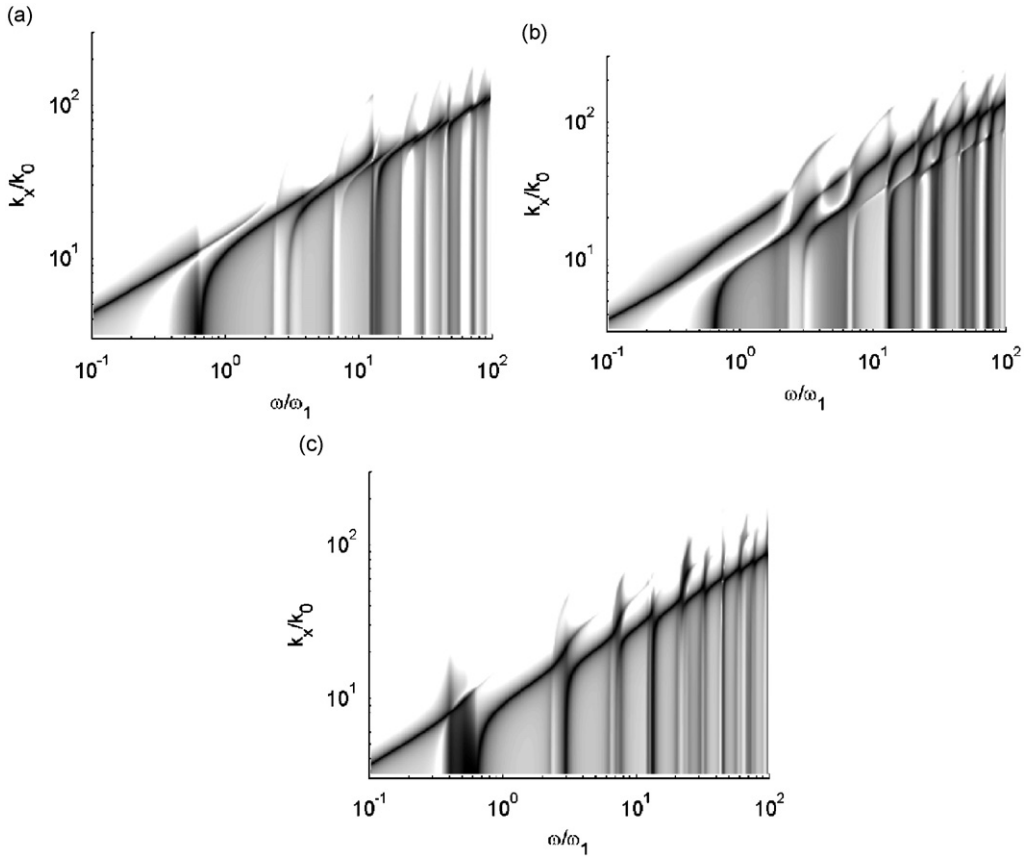

Fig. 11. Magnitude of response in wavenumber–frequency domain of plate with two edge beams, $y = 0.354L_y$. Response normalised to maximum at each frequency, dynamic range 30 dB: (a) identical beams, (b) less stiff beam is driven, and (c) stiffer beam is driven.

the spring-connected case, the transmission to the non-driven beam is generally largest when the beams are identical; for the dissimilar beams it is about a factor of 10 lower when the less stiff beam is driven than when the stiffer beam is driven.

3.7. Influence of beam torsion

Torsion of the beam can be included into the equations of motion. In this case the full 4×4 dynamic stiffness matrix $\mathbf{S}$ in Eq. (20) is retained. The rotations of each beam are included as two additional degrees of freedom $\tilde{\Theta}_{bi}$ in Eq. (7). The matrix $\mathbf{\Gamma}$ in Eq. (7) becomes a 4×4 diagonal matrix with the two additional terms

$$\gamma_{33} = \tilde{G}J_{b1}k_x^2 - m'_{b1}r_1^2\omega^2, \quad \gamma_{44} = \tilde{G}J_{b2}k_x^2 - m'_{b2}r_2^2\omega^2 \tag{24}$$

where $\tilde{G}J_{bi}$ is the torsional rigidity, made complex by including the damping term $(1 + i\eta)$, and r_i is the radius of gyration of the beam.

Fig. 14 shows the mobility components at each wavenumber calculated for the identical beam case. These results are similar to those with the rotation constrained, shown in Fig. 10(a) and (b), except that two waves are present at very low frequency and the cut-on of each subsequent wave is shifted towards higher frequency.

The point mobility of the beam–plate–beam system in the presence of torsion is shown in Fig. 15. Compared with the case in which rotation is constrained, from Fig. 12, the position of the peaks occurring at the cut-on of each wave are shifted in frequency and at higher frequencies they are reduced in amplitude. However, the general level of the mobility follows the same trend as previously.

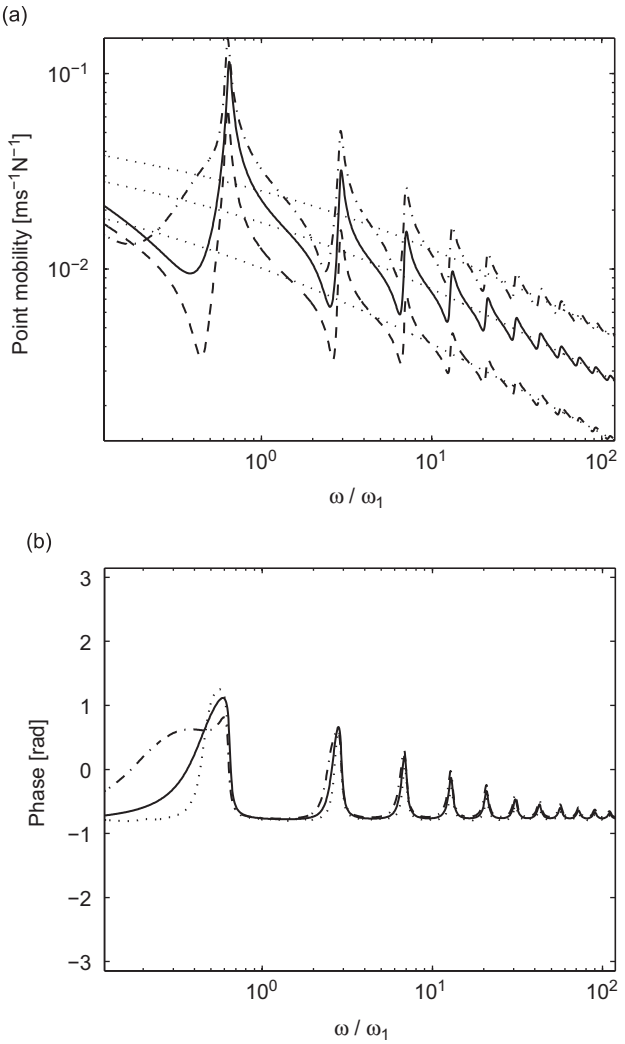

Fig. 12. Point mobility of coupled beam systems: (—) identical beams, (– – –) dissimilar beams (stiffer beam driven), (– · – ·) dissimilar beams (less stiff beam driven), and (· · · · · ·) mobility of equivalent semi-infinite beam–plate systems [22,23].

4. Experimental results

4.1. Experimental arrangement

Measurements have been performed on two different beam–plate–beam structures constructed from acrylic plastic. This material was chosen because of its high damping and relatively low longitudinal wavespeed (1950 m/s). Each consisted of a plate of thickness 2 mm and dimensions $0.5 \times 1.0\,\mathrm{m}^2$ with beams attached along the longer edges. Rectangular sections were attached both above and below the plate with a hard glue to form beams of width 10 mm and height 22, 32 or 52 mm, as shown in Fig. 16. The plate width between the beams was therefore 0.48 m. One structure had identical 32 mm high beams, the other had dissimilar 22 and 52 mm beams. These configurations correspond to the parameters used above and listed in Table 1.

The structures were excited using a shaker attached at the end of one of the beams in the out-of-plane direction. By exciting the structure with dissimilar beams on each beam in turn, a total of three configurations was realised. The force was measured using a force transducer and the velocity of the plate and both beams was measured by using a scanning laser vibrometer in the frequency range 10–1000 Hz ($\omega/\omega_1 = 1.2$–120).

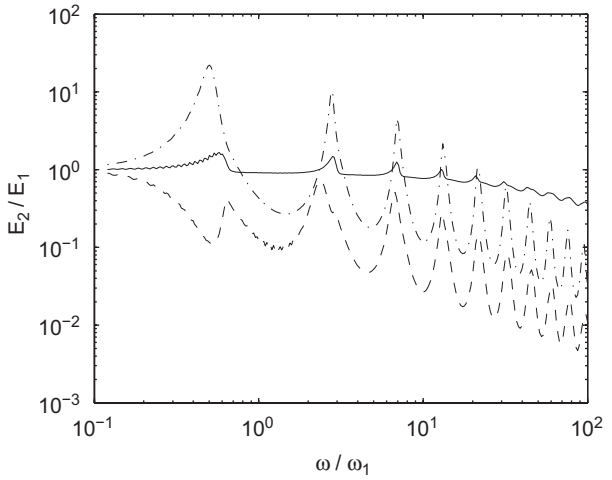

Fig. 13. Ratio of total energy in non-driven beam to that in driven beam for two beams connected by a plate: (—) identical beams, (– · – ·) stiffer beam driven, and (– – –) less stiff beam driven.

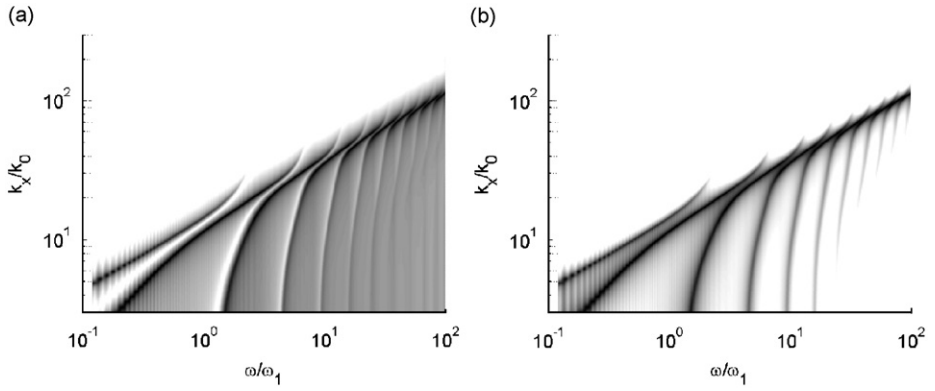

Fig. 14. Magnitude of response in wavenumber–frequency domain of identical two beams connected by plate with beams free to rotate. Response normalised to maximum at each frequency, dynamic range 30 dB: (a) on driven beam and (b) on non-driven beam.

A rectangular grid of measurement points was used on the plates with a spacing of approximately 25 mm. This corresponds to at least three points per plate wavelength at the maximum frequency of interest.

The damping loss factors were measured on plate strips and beams of the same material, the beams being constructed using the same glue as here. These plate strips and beams each had only six resonances in the range 50–1000 Hz so that the damping could be determined simply by finding the half power bandwidth. The loss factors were found to vary from about 0.07 at 50 Hz to 0.04 at 1000 Hz [23].

4.2. Spatial response

The response measured on the structure could be animated and was found to show propagating wavefronts particularly at higher frequencies. Examples are shown in Fig. 17 for the case of dissimilar beams excited on the stiffer beam at 500 and 1000 Hz ($\omega/\omega_1 = 60$ and 120). This shows a comparison of measured and predicted results in the form of the real part of the mobility, which is a snapshot of the response. The predictions are obtained from the inverse Fourier transform of the solution in the wavenumber domain. The system was excited at the bottom left-hand corner. In each case dashed lines have been added to indicate approximately the wavefronts, which can be seen to propagate at a similar angle relative to the beam. This angle is such that

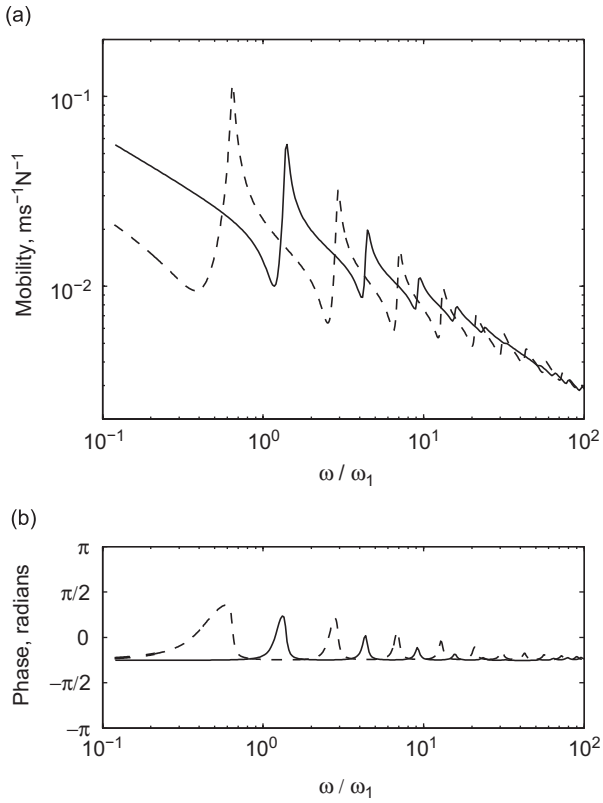

Fig. 15. Point mobility of coupled beam-plate system with two identical beams: (—) with beams free to rotate and (– – –) with beams constrained to prevent rotation.

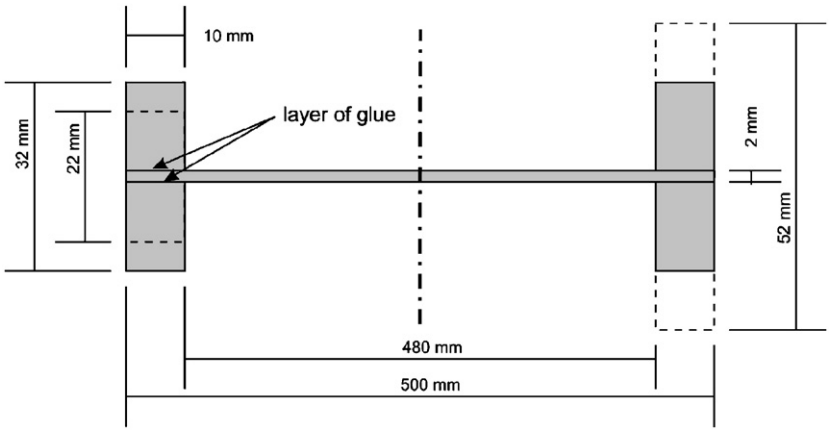

Fig. 16. Sketch of test specimen cross-section.

the corresponding wavelength along the beam is considerably longer than that across the plate. Quite good agreement is seen between measurements and predictions in terms of the direction of these wavefronts and the wavelength (distance between wavefronts).

Although these spatial responses show the wave propagation visually, it is of more value to analyse the measured results in terms of the wavenumber components.

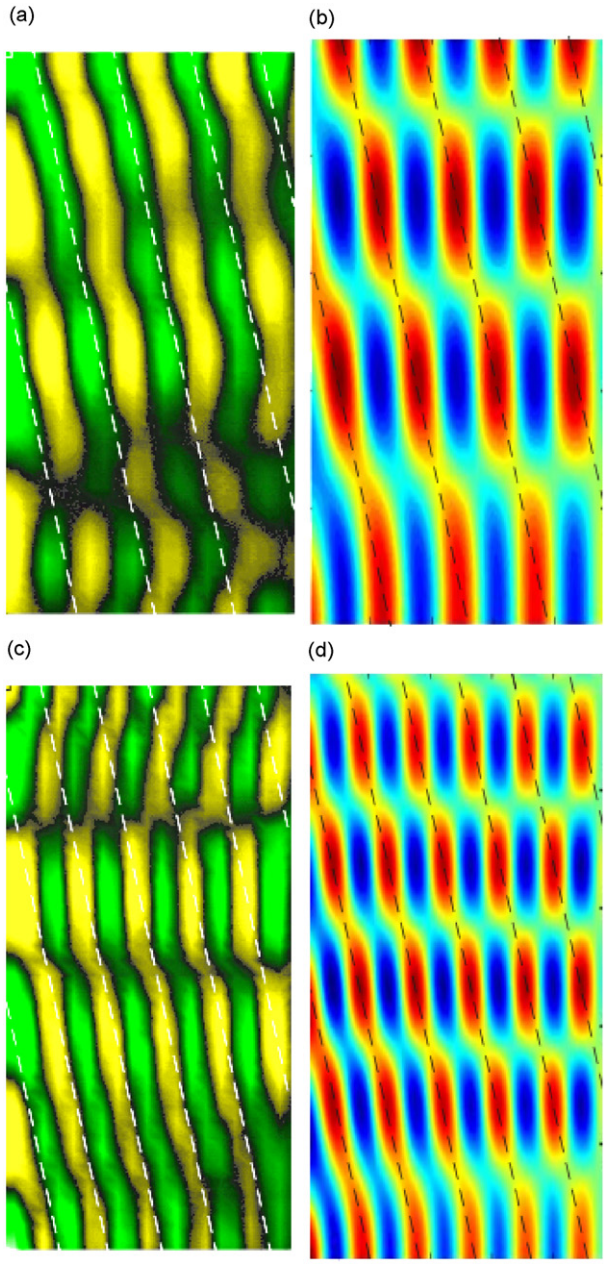

Fig. 17. Comparison of measured (left) and predicted (right) real part of transfer mobility for 52-2-22 mm case: (a,b) at 500 Hz, and (c,d) at 1000 Hz. Diagonal lines have been added to indicate wavefronts.

4.3. Wavenumber estimation

The 2D correlation method described by Ferguson et al. [19,20] has been used to estimate the dominant wavenumbers in the x and y directions from the measured responses. In Cartesian coordinates the 2D correlation function at a single frequency and for discrete samples is given by

$$\tilde{C}(k_x, k_y) = \frac{L_x L_y}{N_x N_y} \sum_{n=1}^{N_x} \sum_{m=1}^{N_y} \tilde{w}(x_n, y_m)\, \mathrm{e}^{-\mathrm{i}k_x x_n}\, \mathrm{e}^{-\mathrm{i}k_y y_m}, \tag{25}$$

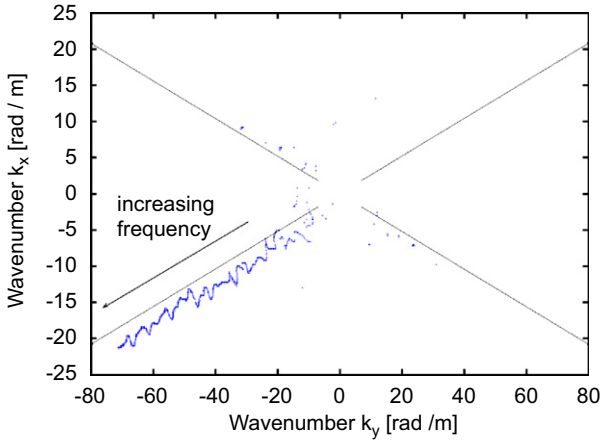

Fig. 18. Wavenumbers extracted from correlation method on 32-2-32 mm specimen. The solid lines correspond to $k_x/k_y = \pm k_b/k_p$.

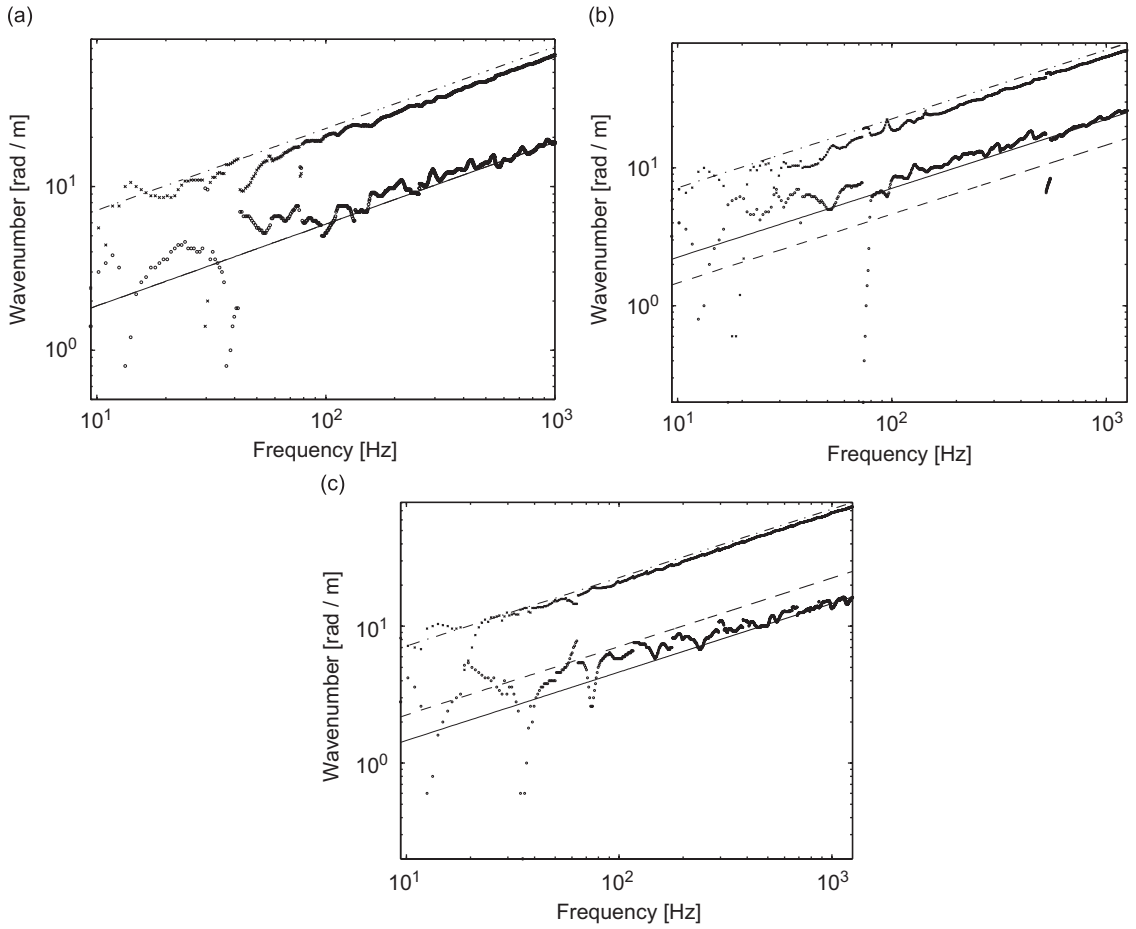

Fig. 19. Wavenumber components k_x and k_y extracted from correlation method: (– · – ·) free wavenumber in plate, (—) free wavenumber in driven beam, (– – –) free wavenumber in non-driven beam, and wavenumbers of coupled system: (×) k_y, (o) k_x. (a) 32-2-32 mm, (b) 22-2-52 mm, and (c) 52-2-22 mm.

where $\tilde{w}$ is the complex response amplitude at positions (x_n, y_m). This function was determined for wavenumbers (k_x, k_y) in the range -25 to $+25$ rad/m along the beam direction and -80 to $+80$ rad/m across the plate, with a resolution of 0.2 rad/m. At each frequency the wavenumber pair (k_x, k_y) giving the maximum value of $|\tilde{C}|$ was extracted.

The results for the case with identical beams are shown in Fig. 18. As can be seen, at most frequencies the dominant component occurred with negative k_x and k_y, corresponding to a wave propagating in the positive x and y directions away from the excitation point. Moreover, the dominant direction of propagation was always the same, with k_y approximately four times k_x. For an infinite isotropic plate it would be expected that wavenumbers would be equally likely to occur for all combinations of k_x and k_y such that $\sqrt{k_x^2 + k_y^2} = k_p$, i.e. points on a circle for a given frequency. Here, however, the driven beam imposes its wavenumber on the system in the x-direction and k_x/k_y is approximately in the ratio k_b/k_p.

These values of k_x and k_y are plotted against frequency in Fig. 19(a). Above 100 Hz the wavenumber components k_x and k_y closely follow the free wavenumbers of the beam and plate, respectively. At low frequency there is a larger variation, which is due partly to the limited length available for the correlation method. Wavenumbers k_x less than 6 rad/m or k_y less than 12 rad/m are not expected to be reliable as the corresponding wavelengths become greater than the dimensions of the structure. Moreover, the limited size of the structure also means that modal behaviour is stronger at these lower frequencies, so the structure behaves less like an infinite waveguide than at higher frequencies.

Equivalent results for the cases with dissimilar beams are shown in Fig. 19(b) and (c). In each case the wavenumber component k_y follows closely the free wavenumber of the plate while k_x tends to follow the free wavenumber of the driven beam, thus showing good agreement with the theoretical results.

The correlation method has also been applied to responses measured on the beams alone [21]. It was found that the response of the driven beam in each case was dominated by the same wavenumbers k_x as found on the plate. The response of the non-driven beam was mostly found to follow the uncoupled wavenumber of the stiffer beam at high frequencies, supporting the predictions in Fig. 11.

5. Conclusions

A beam–plate–beam system has been studied as a structural waveguide using analytical models and a Fourier transform approach. It has been shown that multiple waves occur in the longitudinal direction, the number of waves at a given frequency depending on the number of modes of the equivalent cross-section occurring below that frequency. However, if the system is excited on one of the beams, the response on the plate and the driven beam is dominated by the waves with a wavenumber component in the x-direction that is close to that of the driven beam. The response of the non-driven beam is dominated by waves that are close to the free wavenumber of the stiffer beam, whether this is driven or not.

The ratio of vibration energy in the non-driven beam to that in the driven beam is greatest when the beams are identical. For non-identical beams, it is smaller when the more flexible beam is driven than when the stiffer beam is driven. Similar behaviour is found for two beams coupled by a resilient layer.

Most results have been obtained with beam torsion suppressed but when it is included in the model the results are generally similar, the main difference being a shift in the wave cut-on frequencies.

Experimental results have been obtained on beam–plate–beam systems with identical and non-identical beams. A correlation technique has been used to extract the dominant wavenumbers in the x and y directions. These results show good agreement with the predictions despite the finite length of the samples and confirm that the plate response consists of waves with wavenumbers in the beam direction that closely follow those of the excited beam.

References

[1] P.M. Morse, K.U. Ingard, *Theoretical Acoustics*, Princeton University Press, Princeton, NJ, USA, 1986, p. 492ff.
[2] P.C. Clemmow, *An Introduction to Electromagnetic Theory*, Cambridge University Press, Cambridge, UK, 1973, p. 189ff.
[3] L. Cremer, M. Heckl, E.E. Ungar, *Structure-borne Sound*, second ed., Springer, Berlin, 1988, pp. 305–309, 450–462.

[4] E. Kausel, J.M. Roësset, Stiffness matrices for layered soils, *Bulletin of the Seismological Society of America* 71 (1981) 1743–1761.
[5] X. Sheng, C.J.C. Jones, M. Petyt, Ground vibration generated by a harmonic load acting on a railway track, *Journal of Sound and Vibration* 225 (1999) 3–28.
[6] L. Ji, Mid-frequency Vibration Analysis of Complex Built-up Structures, Ph.D. Thesis, University of Southampton, 2003.
[7] L. Ji, B.R. Mace, R.J. Pinnington, A hybrid/Fourier transform approach to estimating the vibration of beam–stiffened plates systems, *Journal of Sound and Vibration* 274 (2003) 547–565.
[8] B. Aalami, Waves in prismatic guides of arbitrary cross-section, *Journal of Applied Mechanics* 40 (1973) 1067–1072.
[9] L. Gavric, Finite element computation of dispersion properties of thin-walled waveguides, *Journal of Sound and Vibration* 173 (1994) 113–124.
[10] S. Finnveden, Evaluation of modal density and group velocity by a finite element method, *Journal of Sound and Vibration* 273 (2004) 51–75.
[11] J.F. Doyle, *Wave Propagation in Structures*, Springer, New York, 1997.
[12] L. Gavric, Computation of propagative waves in free rail using a finite element technique, *Journal of Sound and Vibration* 185 (1995) 531–543.
[13] I. Bartoli, A. Marzani, F. Lanza di Scalea, E. Viola, Modeling wave propagation in damped waveguides of arbitrary cross-section, *Journal of Sound and Vibration* 295 (2006) 685–707.
[14] S. Finnveden, Spectral finite element analysis of the vibration of straight fluid-filled pipes with flanges, *Journal of Sound and Vibration* 199 (1997) 125–154.
[15] C.-M. Nilsson, Waveguide Finite Elements Applied on a Car Tyre, Ph.D. Thesis, KTH, Stockholm, Sweden, 2004.
[16] B.R. Mace, D. Duhamel, M.J. Brennan, L. Hinke, Finite element prediction of wave motion in structural waveguides, *Journal of the Acoustical Society of America* 117 (2005) 2835–2843.
[17] D.J. Thompson, Wheel–rail noise generation, part III: rail vibration, *Journal of Sound and Vibration* 161 (1993) 421–446.
[18] D.J. Mead, Wave propagation and natural modes in periodic systems: II. Multi-coupled systems with and without damping, *Journal of Sound and Vibration* 40 (1975) 19–39.
[19] N.S. Ferguson, C.R. Halkyard, B.R. Mace, K.H. Heron, The estimation of wavenumbers in two-dimensional structures, *Proceedings of the ISMA 2002*, Leuven.
[20] A.N. Thite, N.S. Ferguson, Wavenumber estimation: further study of the correlation technique and use of SVD to improve propagation direction resolution, ISVR Technical Memorandum No. 937, 2004.
[21] J. Rohlfing, Modelling Vibration of Beam–plate–beam Coupled Systems using a Fourier Transform Technique, M.Sc. Dissertation, ISVR, University of Southampton, 2007.
[22] R.M. Grice, R.J. Pinnington, A method for the vibrational analysis of built-up structures, part 1: introduction and analytical analysis of the plate-stiffened beam, *Journal of Sound and Vibration* 230 (1999) 825–849.
[23] J.W. Yoo, Dynamic Modelling of Beam–plate Systems in the Mid-frequency Region, Ph.D. Thesis, University of Southampton, 2005.